Energy and Buildings 128 (2016) 867–875

Contents lists available at ScienceDirect

Energy and Buildings

journal homepage: www.elsevier.com/locate/enbuild

Numerical simulation of particle deposition in duct air flows with uniform, expanding or contracting cross-section

Hao Lu, Lin Lu*, Yu Jiang

Department of Building Services Engineering, The Hong Kong Polytechnic University, Hung Hom, Kowloon, Hong Kong, China

ARTICLE INFO

Article history:
Received 9 March 2016
Received in revised form 25 April 2016
Accepted 25 July 2016
Available online 26 July 2016

Keywords:
Particle deposition
Expanding duct
Contracting duct
Numerical simulation

ABSTRACT

Particle deposition in two-dimensional turbulent duct air flows with uniform, expanding or contracting cross-section was studied by CFD simulation. The Reynolds stress turbulent model (RSM) with UDF correction and discrete particle model (DPM) were adopted to predict air flow fields and particle deposition rate. After numerical validation of air velocity profiles and particle deposition velocity in uniform duct, the air flow field structures, flow drag and particle deposition behaviors in expanding and contracting ducts with different air velocities and particle sizes were investigated and compared with uniform duct case. It was found that particle deposition velocity is overall reduced in expanding duct while enhanced in contracting duct. However, the modification magnitude of deposition velocity is significant discrepant for different particle sizes due to the role of near-wall turbulent eddies. For expanding duct cases, the particle deposition velocities are reduced about one or two orders of magnitude for large particles ($d_p > 3\mu m$) but less than 5 times for small particles ($d_p < 3\mu m$), compared with uniform duct cases. For contracting duct cases, the particle deposition velocities are increased less than 7 times for large particles while about 20–60 times for small particles. Besides, the deposition mechanisms of particles in expanding and contracting duct were also studied and discussed.

1. Introduction

Particle deposition and dispersion in duct air flow are significant for environment and energy engineering applications, such as indoor environment quality, pneumatic conveying and pulverized coal combustion [1–6]. Better understanding of particle deposition behaviors in duct is crucial for improving indoor air quality (IAQ) and related equipment efficiency [7–11]. So far, particle deposition in ducts with uniform section has been well investigated by many researchers. Nevertheless, few attentions have been paid on particle deposition in duct with variable cross-section, such as expanding section or contracting section. However, this issue may also be commonly encountered in a large number of energy and environment engineering applications, and need to be studied in details.

For particle deposition in duct air flows with uniform section, a large number of experimental studies were conducted to measure deposition velocity profile with particle relaxation time [12–15]. The results showed that deposition velocity profile in vertical duct flow can be divided into three regimes: turbulent particle diffusion regime, eddy diffusion-impaction regime and inertia-moderated regime. The particle deposition velocity profile would first decrease, and then greatly increase for several orders of magnitude, finally keeps constant or decreases slightly with the increase of particle relaxation time. Theoretical models [15–19] were also developed for fast predicting particle deposition rate in practical engineering application. Lai and Nazaroff [17] proposed the three-layer model to predict particle deposition velocity on smooth surface by considering gravitational settling, Brownian and turbulent diffusion. This model was further developed by Zhao and Wu [18,19] to successfully predict particle deposition velocity in ventilation duct with smooth and rough walls. In recent years, numerical simulation based on CFD method has become a powerful tool to investigate particle deposition process in various engineering problems [20–23]. Many numerical investigations have been carried out to successfully predict particle deposition in duct air flows with uniform section [24–28]. The Eulerian-Lagrangian approaches were usually applied to simulate particle deposition process in duct air flow [29]. Tian and Ahmadi [30] predicted particle deposition rate in duct air flows by different turbulent models. They found that Reynolds Stress model with turbulent fluctuation correction can simulate particle deposition velocity more accurately, compared with other RANS model. Zhang and Chen [31] proposed a modified Lagrangian method to predict particle deposition in turbulent

* Corresponding author.
E-mail address: vivien.lu@polyu.edu.hk (L. Lu).

http://dx.doi.org/10.1016/j.enbuild.2016.07.052
0378-7788/

Nomenclature

C_0	Mean particle concentration
D_1	Uniform duct width
D_2	Outlet width of expanding duct
D_3	Outlet width of contracting duct
F_S	Saffman's lift force
f	Fanning friction factor
h	Duct height
J	Number of particles deposited per unit time and unit area
k	Turbulent kinetic energy (T.K.E.)
$\bar{p}$	Time-averaged pressure
Re	Reynolds number
S	Ratio of particle-to-fluid density
U_{mean}	Mean velocity of air
U_{free}	Freestream velocity of air
u_g	Velocity of fluid
$\bar{u}_i$	Time-averaged velocity
u_p	Velocity of particle
u'_{rms}	Streamwise fluctuating velocity of air
V_d	Particle deposition velocity
V_d^+	Dimensionless particle deposition velocity
v'_{rms}	Wall-normal fluctuating velocity of air
w'_{rms}	Spanwise fluctuating velocity of air
u^*	Frictional velocity of air
y^+	Dimensionless distance from the wall

Greek symbols

ε	Dissipation rate of turbulent kinetic energy
ρ_g	Density of fluid
ρ_p	Density of particle
ζ	Normal distributed random number
μ	Dynamic viscosity of air
ν	Kinetic viscosity of air
τ_p^+	Dimensionless particle relaxation time

duct flow. The results showed that near-wall turbulence effect is important for particle deposition behaviors.

However, very few studies have been conducted for particle deposition in duct air flows with variable cross-section. Sippola and Nazaroff [32–34] detailedly measured particle deposition in straight duct, S-connector and duct bend. They found that particle deposition rate in S-connector and duct bend are greater than that in straight ducts. Particle transport and deposition in expanding and contracting alveolus were numerically investigated by Haber et al. and Lee et al. [35,36]. It was found that near-wall motion is crucial for the enhancement of aerosol deposition inside the alveoli. Nevertheless, the alveolus configuration and flow structure are greatly different with duct flows. In the authors' previous studies, particle deposition in ribbed duct air flow with different rib heights, spacing and shapes were investigated by CFD simulation [2,20,22]. The results showed that particle deposition behavior and velocity are significantly modified because of the variation of duct section configuration. In this study, the particle deposition in expanding and contracting duct air flows were investigated by CFD method and compared with uniform section duct case. The Reynolds stress model (RSM) with turbulent fluctuation correction and discrete particle model (DPM) were employed to predict air flow fields and particle deposition behaviors. Particle deposition velocity with different sizes, flow field structures, flow drag and deposition mechanisms in expanding and contracting ducts were analyzed and discussed.

2. Numerical models and solution methods

In this study, Eulerian-Lagrangian approaches were adopted to simulate particle deposition process in turbulent duct air flows. The Reynolds stress model (RSM) with near-wall correction and discrete particle model (DPM) were employed to predict air flow fields and particle deposition behaviors, respectively. The simulation was conducted based on the commercial software ANSYS FLUENT with UDF codes.

2.1. Turbulent air flow model with near-wall correction

To resolve the turbulent duct air flow fields, the mass conservation governing equation is described by,

$$\frac{\partial \bar{u}_i}{\partial x_i} = 0, \tag{1}$$

The momentum conservation governing equation is demonstrated as follow,

$$\frac{\partial \bar{u}_i}{\partial t} + \bar{u}_j \frac{\partial \bar{u}_i}{\partial x_j} = -\frac{1}{\rho}\frac{\partial \bar{p}}{\partial x_i} + \frac{1}{\rho}\frac{\partial}{\partial x_j}\left(\mu \frac{\partial \bar{u}_i}{\partial x_j} - \rho \overline{u'_i u'_j}\right), \tag{2}$$

In Eqs. (1) and (2), $\bar{u}_i$is the time-averaged velocity. $\bar{p}$is the time-averaged pressure. $\rho\overline{u'_i u'_j}$is the Reynolds stress tensor.

The RSM model was adopted to close the above Reynolds-Averaged Navier-Stokes equations. The Reynolds stress transport equation can be described by,

$$\frac{\partial}{\partial t}(\overline{u'_i u'_j}) + \bar{u}_k \frac{\partial}{\partial x_k}(\overline{u'_i u'_j}) = \underbrace{\frac{\partial}{\partial x_k}\left(\frac{\nu_t}{\sigma_k}\frac{\partial \overline{u'_i u'_j}}{\partial x_k}\right)}_{D_{T,ij}=TurbulentDiffusion} \underbrace{-\left(\overline{u'_i u'_k}\frac{\partial \bar{u}_j}{\partial x_k} + \overline{u'_j u'_k}\frac{\partial \bar{u}_i}{\partial x_k}\right)}_{P_{ij}=StressProduction} \underbrace{-C_1\frac{\varepsilon}{k}\left[\overline{u'_i u'_j} - \frac{2}{3}\delta_{ij}k\right] - C_2\left[P_{ij} - \frac{2}{3}\delta_{ij}P\right]}_{\phi_{ij}=PressureStrain} \underbrace{-\frac{2}{3}\delta_{ij}\varepsilon}_{\varepsilon_{ij}=Dissipation} \tag{3}$$

The two-layer zonal model with enhanced wall function was employed to deal with near-wall turbulent flow fields in the simulation [30]. The previous studies [29–31] showed that the wall-normal turbulent velocity fluctuation has great influence on particle deposition behaviors. The RSM model without near-wall turbulent fluctuation correction would over-predict the deposition velocity in the diffusion-impaction regime. In this study, RSM model with wall-normal turbulent velocity fluctuation correction was adopted to predict particle deposition in uniform, expanding and contracting duct air flows. To correct the near-wall turbulent velocity fluctuation in the wall-normal direction, the direct numerical simulation (DNS) data by Kim et al. [37] in uniform duct flow was employed and imposed in FLUENT by UDF codes, as follows,

$$\frac{v'_{rms}}{u^*} = C(y^+)^2, \text{ for } y^+ < 4 \tag{4}$$

For expanding and contracting duct cases, the correction Eq. (5) was adopted in the near-wall region. This correction was successfully applied in predicting aerosol deposition in a human mouth geometry by Dehbi [38] and ribbed duct by Lecrivain et al. [39]. It can be described by,

$$\frac{v'_{rms}}{u^*} = \frac{a_1 y^{+2}}{1 + b_1 y^+ + c_1 y^{+2.41}}, \text{ for } y^+ < 30 \tag{5}$$

In Eq. (4) and (5), $C = 0.008$,$a_1 = 0.0116$,$b_1 = 0.203$ and $c_1 = 0.0014$. $u^*$is the friction velocity. $y^+$is the non-dimensional distance from the wall, which can be defined by,

$$y^+ = \frac{y u^*}{\nu} \tag{6}$$

2.2. Particle motion model with turbulent particle dispersion

Particle movements were simulated by discrete particle model (DPM) in Lagrangian frame. In the present study, the air-particle flow is so dilute that the modification of particle on air flow fields and particle–particle collision can be neglected. The particle governing equation can be described as follows,

$$\frac{du_p}{dt} = \frac{1}{\tau}\frac{C_D Re_p}{24}(u_g - u_p) + \frac{g(\rho_p - \rho_g)}{\rho_p} + \zeta\sqrt{\frac{\pi S_0}{\Delta t}} + \frac{2\rho K_c \nu^{0.5}}{\rho_p d_p (S_{lk} S_{kl})} s_{ij}(u - u_p) \quad (7)$$

The right hand side of the above equation is the drag force term, the gravity and buoyancy force term, the Brownian force term and the Saffman's lift force term. As the ratio of air density to particle density is very small, the pressure gradient force, the Basset force and the virtual mass force can be neglected compared with the above particle forces [40]. The drag coefficient C_D is calculated by,

$$C_D = \frac{24}{Re_p}, \text{ for } Re_p < 1 \quad (8)$$

and

$$C_D = \frac{24}{Re_p}(1 + 0.15 Re_p^{0.687}), \text{ for } 1 < Re_p < 400 \quad (9)$$

The particle relaxation time τ can be calculated by,

$$\tau = \frac{S d_p^2 C_C}{18\nu} \quad (10)$$

where S is the ratio of particle density to fluid density, and C_C is the Cunningham slip correction factor.

Turbulent particle dispersion is crucial to accurately predict the particle deposition velocity [30]. In this study, discrete random walk model was adopted to deal with turbulent dispersion of particles. The DRW model is characterized by a Gaussian distributed random velocity fluctuation of fluids and a time scale of turbulent eddy [41]. The instantaneous turbulent fluctuating velocities are computed as follows,

$$u' = \zeta u'_{rms},\ v' = \zeta v'_{rms},\ w' = \zeta w'_{rms} \quad (11)$$

where u'_{rms}, v'_{rms} and w'_{rms} are the velocity fluctuation and ζ is normal distributed random number.

2.3. Boundary conditions

For air duct flow, the fully developed velocity profiles of one seventh power law were adopted and imposed in the air flow inlet by UDF codes, which can be demonstrated as follows [30],

$$U = U_{free}\left(\frac{y}{D/2}\right)^{1/7}, \text{ for } y \le D/2 \quad (12)$$

$$U = U_{free}\left(\frac{h-y}{D/2}\right)^{1/7}, \text{ for } y > D/2 \quad (13)$$

$$U_{free} = \frac{8}{7}U_{mean} \quad (14)$$

where D is duct inlet height. U_{mean} is mean air velocity. Besides, the fully developed turbulent kinetic energy (T.K.E.) profiles were also employed in the duct inlet as follows [30],

$$k = \frac{\tau_w}{\rho_g\sqrt{C_\mu}} + \frac{y}{D/2}\left(0.002U_{free}^2 - \frac{\tau_w}{\rho_g\sqrt{C_\mu}}\right) \text{ for } 0 \le y \le D/2 \quad (15)$$

$$k = \frac{\tau_w}{\rho_g\sqrt{C_\mu}} + \frac{D-y}{D/2}\left(0.002U_{free}^2 - \frac{\tau_w}{\rho_g\sqrt{C_\mu}}\right) \text{ for } D/2 < y \le D \quad (16)$$

$$\tau_w = \frac{\rho_g U_{mean}^2}{2}\cdot f \quad (17)$$

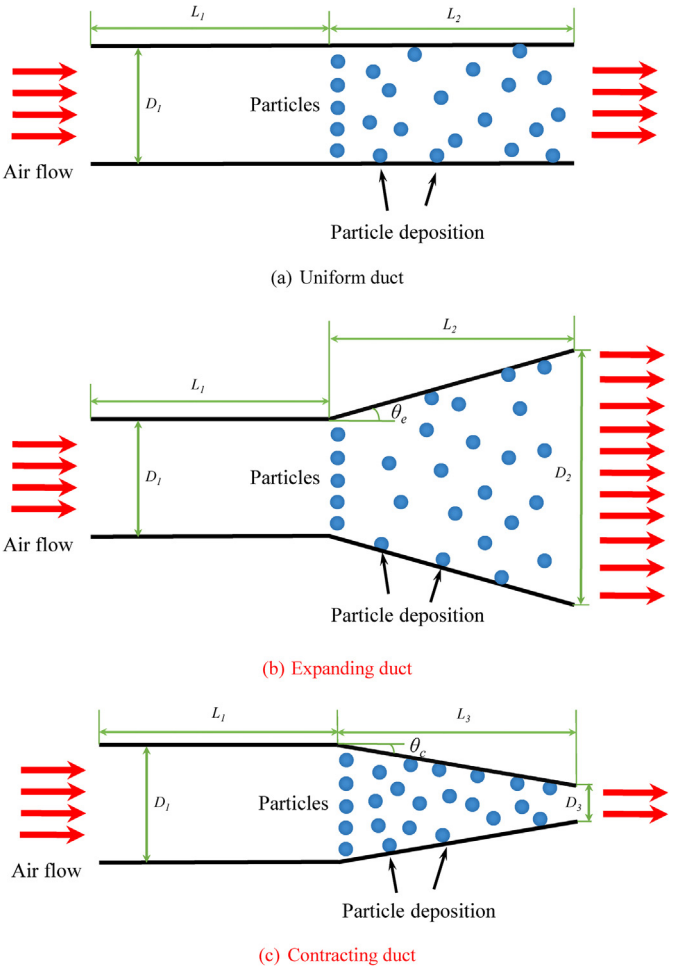

Fig. 1. Schematic view of particle deposition in uniform, expanding and contracting ducts.

Pressure outlet condition was adopted at the air flow outlet. The non-slip condition was used on the duct walls. For particle motion, it was assumed that the particles would not be rebound and re-suspended from the walls. All the particles will be attached to the duct walls and never be re-suspended once they impact on the walls [29–31].

2.4. Solution methods

The governing equations of air duct flow were resolved by the finite volume method (FVM). The particle motion governing equations were resolve by the Runge-Kutta method. The pressure and velocity fields were decoupled by the SIMPLE algorithm [42]. The convection term and the diffusion term were discretized by the second-order upwind scheme and the second-order central difference scheme. The turbulent velocity fluctuation correction and fully developed velocity and T.K.E. profiles were imposed into FLUENT by UDF codes.

3. Case description

3.1. Computational cases

The schematic view of particle deposition in uniform, expanding and contracting ducts is displayed in Fig. 1(a)–(c). The uniform duct is 0.4 m in length and 0.02 m in width. This design is in consistent with Tian and Ahmadi [30] as well as Zhang and Chen [31] for

Table 1
Computational cases.

Case No.	Air velocity (m/s)	Particle diameter (μm)	Duct Type
S (1–16)	5.5 m/s, 8 m/s	1,2,3,5,10,20,30,50	Uniform
E (17–32)	5.5 m/s, 8 m/s	1,2,3,5,10,20,30,50	Expanding
C (33–48)	5.5 m/s, 8 m/s	1,2,3,5,10,20,30,50	Contracting

further comparison. For expanding and contracting ducts, the duct width starts to vary at the mid-section of the duct. The expanding ratio of duct width D_1/D_2 is 1:2 and the contracting ratio D_1/D_3 is 2:1. The corresponding expanding angle of duct width θ_e is 2.86° and the contracting angle θ_c is 1.43°, as shown in Fig. 1 (b) and (c), respectively. In this study, the air velocities were designed as 5.5 m/s and 8m/s. The air dynamic viscosity μ is 1.789×10^{-5} kg s/m. The air density is 1.225 kg/m^3 at T = 288 K. When the air flow fields reached calculation convergence, typical 30,000 spherical particles were released with a uniform distribution at the streamwise middle position of the duct (L_1 = 0.2 m and L_2 = 0.2 m in Fig. 1). The initial velocities of particles were equal to the mean velocity of the air flow. The density ratio of particle to fluid S is 2000. Eight particle sizes (1, 2, 3, 5, 10, 20, 30 and 50 μm) were investigated in the simulation. The detailed computational cases can be seen in Table.1.

3.2. Structured grids

The structured grids were developed by ANSYS ICEM 13.0 to discretize the calculation domain for uniform, expanding and contracting ducts. For particle deposition simulation in uniform duct, very detailed grid independence test had be conducted by Tian and Ahmadi [30]. They investigated the influences of several different grid solutions and first grid spacings from the duct wall on the prediction results. The results showed that the accurate prediction compared with experimental data can be obtained when the first grid spacing is 0.05 mm and the grid growing factor was 1.2 from the walls to the core regions. In this study, the grid independence check was not conducted repeatedly. This grid solution of Tian and Ahmadi [30] was adopted in this paper. For uniform duct, the whole computational grid number is 32,000. For expanding and contracting ducts, the grid numbers are both 32,000. The partial enlarged computational grids are showed in Fig. 2(a)–(c).

4. Results and discussions

4.1. Numerical validation

First, the mean and fluctuating velocity profiles of air flow in uniform duct were validated with DNS data by Kim et al. [37], as shown in Fig. 3(a) and (b), respectively. It can be seen that the mean velocity profile is in good agreement with the DNS result. From Fig. 3(b), the streamwise fluctuating velocity profile agrees roughly with the DNS data. Nevertheless, the wall-normal fluctuating velocity profile agrees much better with the literature results after near-wall correction. As the wall-normal turbulent fluctuating velocity is crucial for predicting particle deposition rate, Fig. 2(c) shows near-wall turbulent velocity fluctuation with and without correction in the wall-normal direction. It can be observed that the RSM model without near-wall correction obviously over-predicts wall-normal fluctuating velocity. This indicates that the near-wall correction of turbulent fluctuation is necessary for the RSM model. The above validation implies that the present RSM model with near-wall correction as well as the grid solution can predict turbulent duct air flow fields very well.

Moreover, particle deposition velocity in uniform duct was predicted and compared with the related literature results

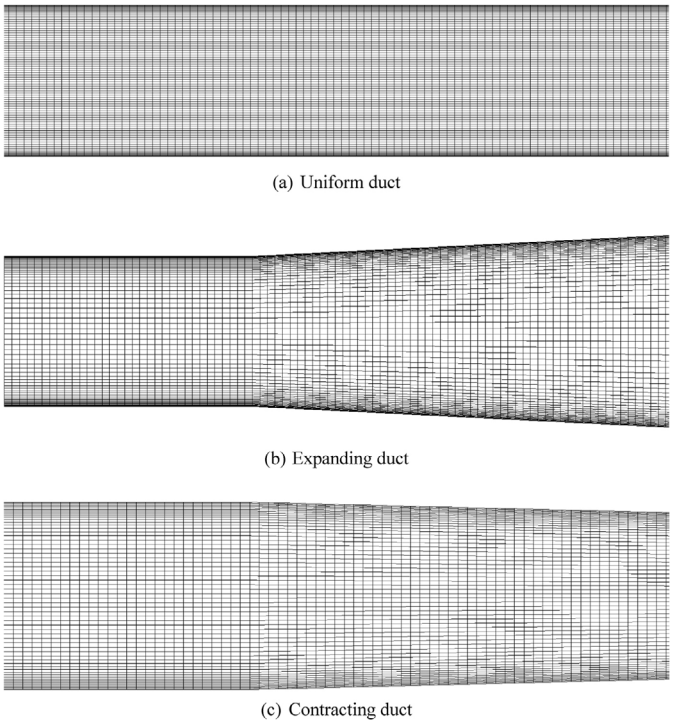

(a) Uniform duct

(b) Expanding duct

(c) Contracting duct

Fig. 2. Partial structural grids for uniform, expanding and contracting ducts.

[12–15,30,31,43–45], as showed in Fig. 4. The particle deposition velocity can be estimated by [30,31],

$$V_d = \frac{J}{C_0} = \frac{N_d/t/A}{N_0/V} \tag{18}$$

where J is deposited particle number per unit time and unit surface area and C_0 is particle mean concentration. The particle deposition velocity is non-dimensionalized by the friction velocity u^*. From Fig. 4, It can be seen that the RSM model with near-wall correction can predict particle deposition velocity accurately. Nevertheless, the RSM model without near-wall correction would over-predict particle deposition rate for small particles ($\tau_p^+ < 1$). These results are in consistent with literatures [30,31]. The eddy diffusion-impaction regime and inertia-moderated regime are both predicted in present study. In the further regime, particle deposition behaviors are determined by turbulent diffusion and particle inertia. However, particle inertia becomes the main mechanism for deposition in the latter regime. The agreement of particle deposition velocity in Fig. 4 indicates that the present numerical models can correctly predict particle deposition process in turbulent duct air flow.

4.2. Particle deposition velocity

Fig. 5 shows particle deposition velocity in uniform, expanding and contracting ducts at 5 m/s. From the figure, it can be seen that particle deposition behaviors are quite different in duct with varying cross-section, compared with the uniform duct case. For expanding duct case, the particle deposition velocities are overall lower than those of uniform duct case for about one or two orders of magnitude. As deposited distance is increased, the expanding duct is obviously against for particle deposition. Moreover, the whole curve shape of deposition velocity is also modified compared with uniform duct case. It is notable that the deposition velocity differences of small particles ($d_p < 3\mu m$) between expanding and uniform ducts are obviously smaller than those of large particles ($d_p > 3\mu m$). For small particles ($d_p < 3\mu m$), the particle

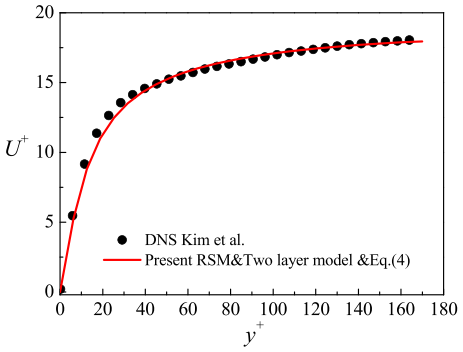

(a) Mean air flow velocity

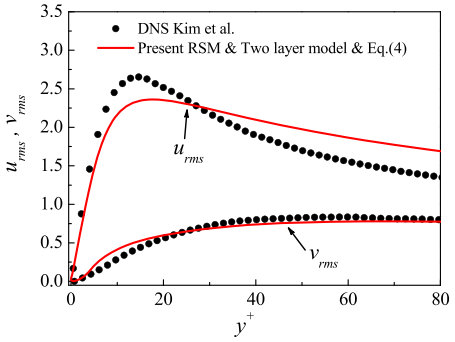

(b) Turbulent fluctuating velocity

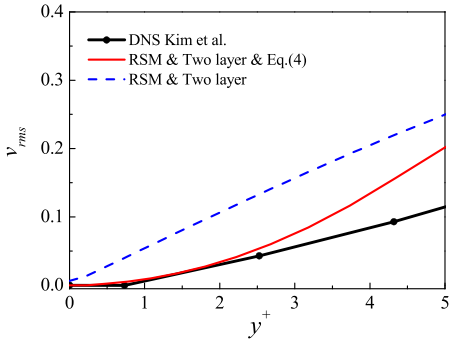

(c) Wall-normal turbulent velocity fluctuation correction

Fig. 3. Validation of velocity profiles for uniform duct flow with DNS data.

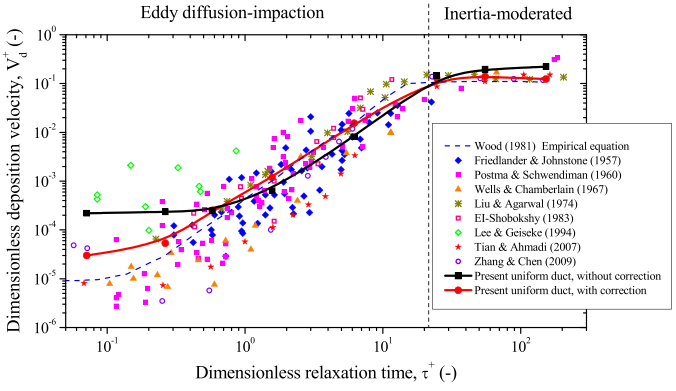

Fig. 4. Dimensionless particle deposition velocity in uniform duct air flow.

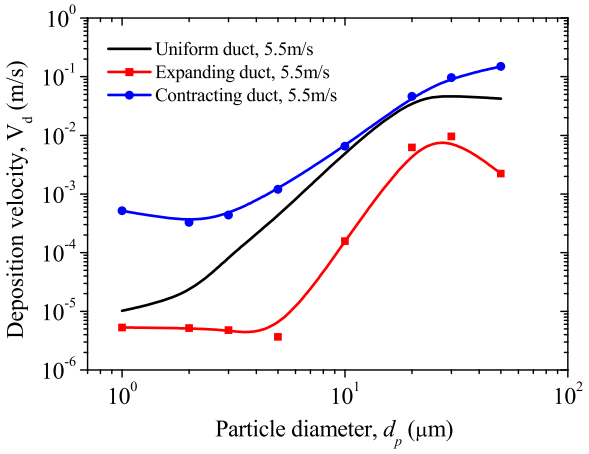

Fig. 5. Particle deposition velocity in uniform, expanding and contracting ducts at 5.5 m/s.

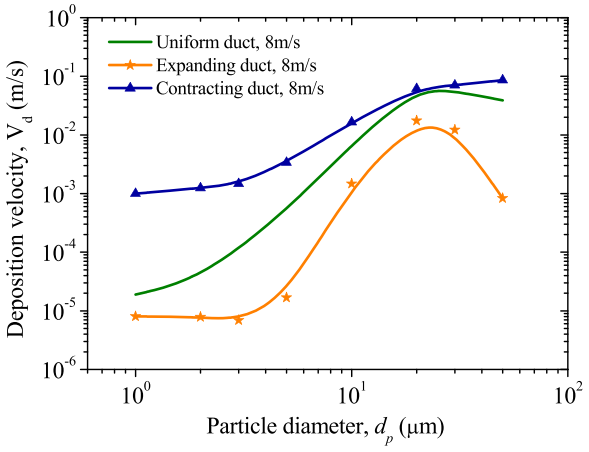

Fig. 6. Particle deposition velocity in uniform, expanding and contracting ducts at 8 m/s.

deposition velocities for expanding duct cases are only decreased for 2–4 times compared with the uniform duct cases. This may be closely related to the flow field structures and turbulent kinetic energy (T.K.E.) distribution in expanding duct. The detailed deposition mechanisms would be discussed in the below section alone. On the contrary, particle deposition velocities in contracting duct are higher than those of uniform duct for all the particle sizes. This is because deposited distance is decreased in contracting duct and a large number of particles would be intercepted by the convergent wall surfaces. Similarly with expanding duct, the deposition velocity differences of small particles ($d_p < 3\mu m$) between contracting and uniform ducts are significantly larger than those of large particles ($d_p > 3\mu m$). For large particles ($d_p > 3\mu m$), the particle deposition velocities for contracting duct cases are increased about 1–5 times while the deposition enhancement ratios can reach 20–50 times for small particles ($d_p < 3\mu m$).

To confirm the above conclusions, particle deposition velocity profiles in uniform, expanding and contracting ducts at 8 m/s are displayed in Fig. 6. From the figure, it can be found that the similar conclusions can be completely obtained when air velocity is increased to 8 m/s. For expanding duct cases, the particle deposition velocities are reduced about one or two orders of magnitude for large particles but less than 5 times for small particles, compared with uniform duct cases. For contracting duct cases, the particle deposition velocities are increased less than 7 times for large particles while about 20–60 times for small particles. This indicates

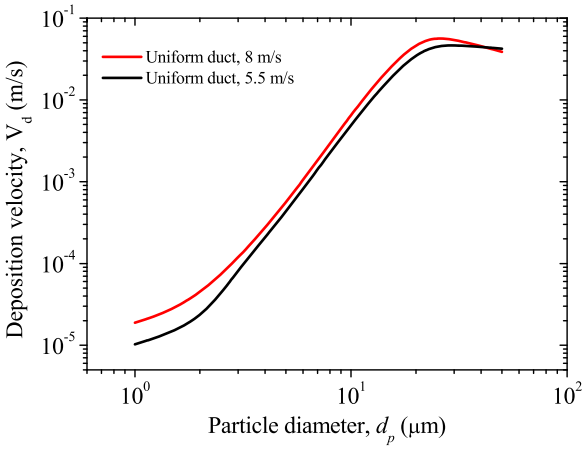

(a) Uniform duct

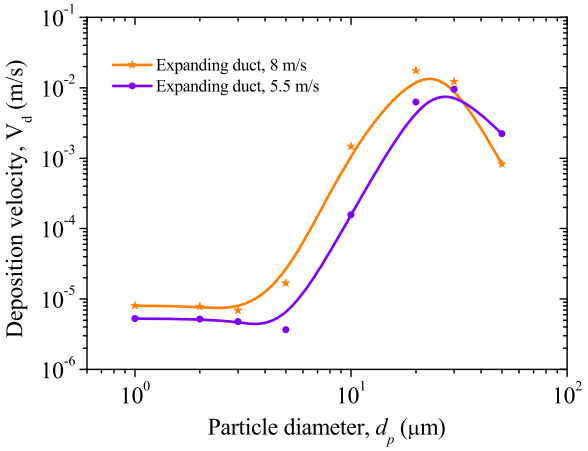

(b) Expanding duct

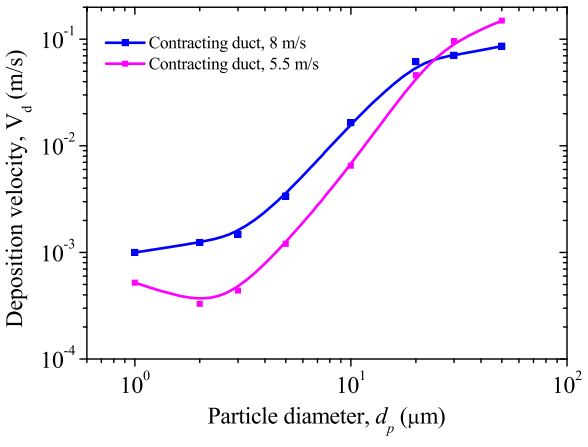

(c) Contracting duct

Fig. 7. Particle deposition velocity in ducts at different air velocities.

that the above conclusions are creditable and independent of flow Reynolds numbers.

It was found that air velocity (friction velocity) has crucial influence on particle deposition rate in uniform duct [18,33]. Generally, the deposition velocity would be increased with the increase of air velocity [18,33]. To investigate the influence of air velocity on particle deposition rate in expanding and contracting ducts, particle deposition velocity profiles at different air velocities for uniform, expanding and contracting ducts are shown in Fig. 7(a)–(c), respectively. For uniform duct case, it can be observed that particle deposition velocity at 8 m/s is slightly higher than that of 5m/s, as shown in Fig. 7(a). This is in consistent with the previous studies [18,33]. For expanding and contracting duct cases, the same conclusions can be obtained from Fig. 7(b) and (c). Nevertheless, the difference of deposition rate between the two air velocities are much larger for expanding and contracting ducts, compared with the uniform duct case. In Fig. 7(a)–(c), it can be found that the curve shapes of deposition velocity are not modified by different air velocities for all types of ducts. This indicates that the deposition mechanisms are the same for different air velocities, although the deposition rate would be increased with the air velocity increase.

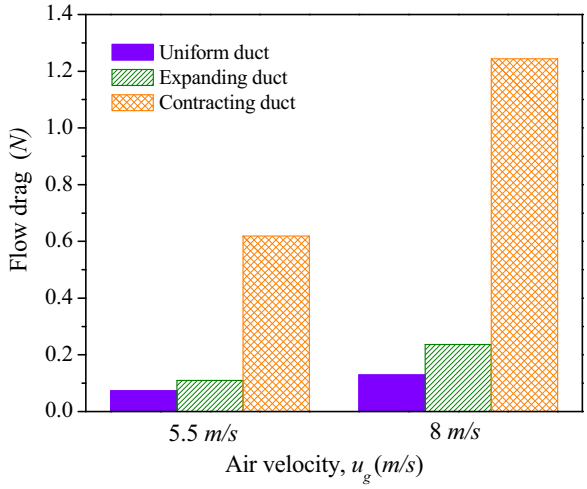

Fig. 8. Flow drags for uniform, expanding and contracting ducts.

4.3. Flow drag

The flow drags were obtained for uniform, expanding and contracting ducts, as shown in Fig. 8. They are 0.0732, 0.1097 and 0.619 N at 5.5 m/s and 0.1289, 0.2361 and 1.2434 N at 8 m/s, respectively. Compared with uniform duct, the flow drags of the expanding and contracting ducts are both increased because of the extra form drag. Moreover, the flow drag is increased by increasing the air velocity for all types of ducts. When air velocity is 5.5 m/s, compared with uniform duct, the flow drag is increased about 1.5 and 8.5 times for expanding duct and contracting duct, respectively. When air velocity is 8 m/s, the increase ratios of flow drag are respectively 1.8 and 9.6 times, which is slightly higher than the case of lower air velocity. The results showed that the flow drag would be greatly increased by contracting cross-section, compared with expanding duct.

4.4. Particle deposition mechanisms

Particle deposition mechanisms would be analyzed and discussed in this section. Firstly, compared with uniform duct case, the deposition distance is obviously increased in expanding duct and decreased in contracting duct. This would directly lead to the reduction of particle deposition rate in expanding duct and particle deposition enhancement in contracting duct.

Secondly, particle deposition behaviors are closely related with the flow field structures, especially for small particles ($d_p < 3\mu m$). Fig. 9 shows air velocity fields for the second half of the uniform, expanding and contracting ducts. From Fig. 9(a), it can be seen that the air velocity distribution remains almost the same along the streamwise direction for the uniform duct. However, the air flow fields become much more complicated in duct with varied

section. The air velocity is obviously decelerated in expanding duct and accelerated in contracting duct in flow direction. The particle deposition behaviors would be modified by the complex flow fields in duct with varying cross-section. As air velocity (friction velocity) can influence particle deposition rate, the deceleration of air velocity in expanding duct would result in the decrease of particle deposition. On the contrary, the acceleration of air velocity and interception of convergent cross-section in contracting duct are also beneficial for particle deposition.

Moreover, from Fig. 5 and Fig. 6, it can be found that the reduction or enhancement degrees are not uniform for different particle sizes. For small particles ($d_p < 3\mu m$), the deposition velocity difference compared with uniform duct case is reduced for expanding duct and enlarged for contracting duct, while it is relatively uniform for large particles ($d_p > 3\mu m$). This may be closely related to flow field structures and near-wall T.K.E. distribution. Fig. 10 shows the T.K.E. distribution and streamlines in uniform, expanding and contracting ducts. It can be observed that the near-wall T.K.E. is significantly more intense for expanding and contracting ducts, as shown in the red regions from Fig. 10(b) and (c). This is much favorable for small particle deposition with low inertia, as these particles are easy to capture by the near-wall flow and deposit on the wall surfaces. Therefore, the deposition velocity difference is reduced for expanding duct but enlarged for contracting duct due to the influence of near-wall turbulent eddies, compared with uniform duct case.

5. Conclusions and outlook

Particle deposition processes in uniform, expanding and contracting ducts were numerically investigated by RSM model with turbulent fluctuation correction and DPM model. The present mean and fluctuating velocity profiles of air flow as well as particle deposition velocity in uniform duct are in good agreement with the previous related studies. Then, particle deposition velocity and mechanisms were studied and analyzed in details. The following conclusions can be drawn,

1 Compared with uniform duct case, particle deposition velocity is lower for expanding duct but higher for contracting duct. However, deposition velocity differences with uniform duct case are quite different between small particles ($d_p < 3\mu m$) and large particles ($d_p > 3\mu m$), both for expanding and contracting ducts. For present expanding duct cases (the expanding angle θ_e is 2.86°), the particle deposition velocities are reduced about one or two orders of magnitude for large particles but less than 5 times for small particles, compared with uniform duct cases. For contracting duct cases (the contracting angle θ_c is 1.43°), the particle deposition velocities are increased less than 7 times for large particles while about 20–60 times for small particles. Moreover, for the three types of duct, particle deposition velocities are all increased with the increase of air velocity.

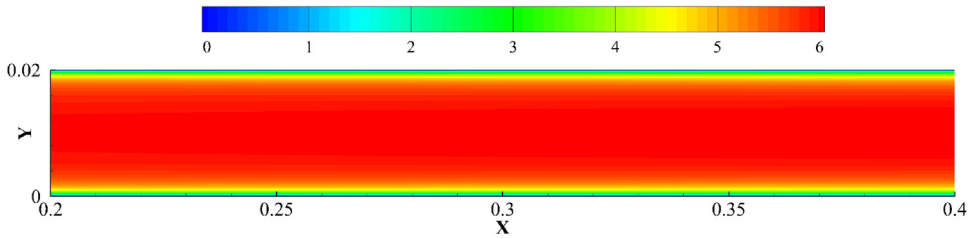

(a) Uniform duct

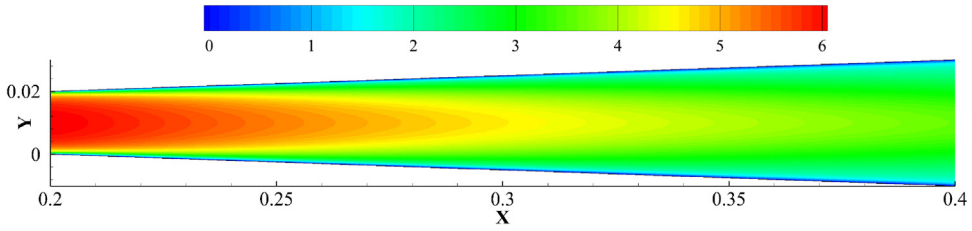

(b) Expanding duct

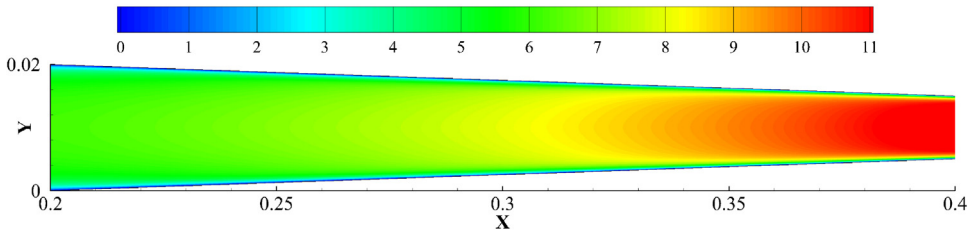

(c) Contracting duct

Fig. 9. Velocity fields of uniform, expanding and contracting duct flows.

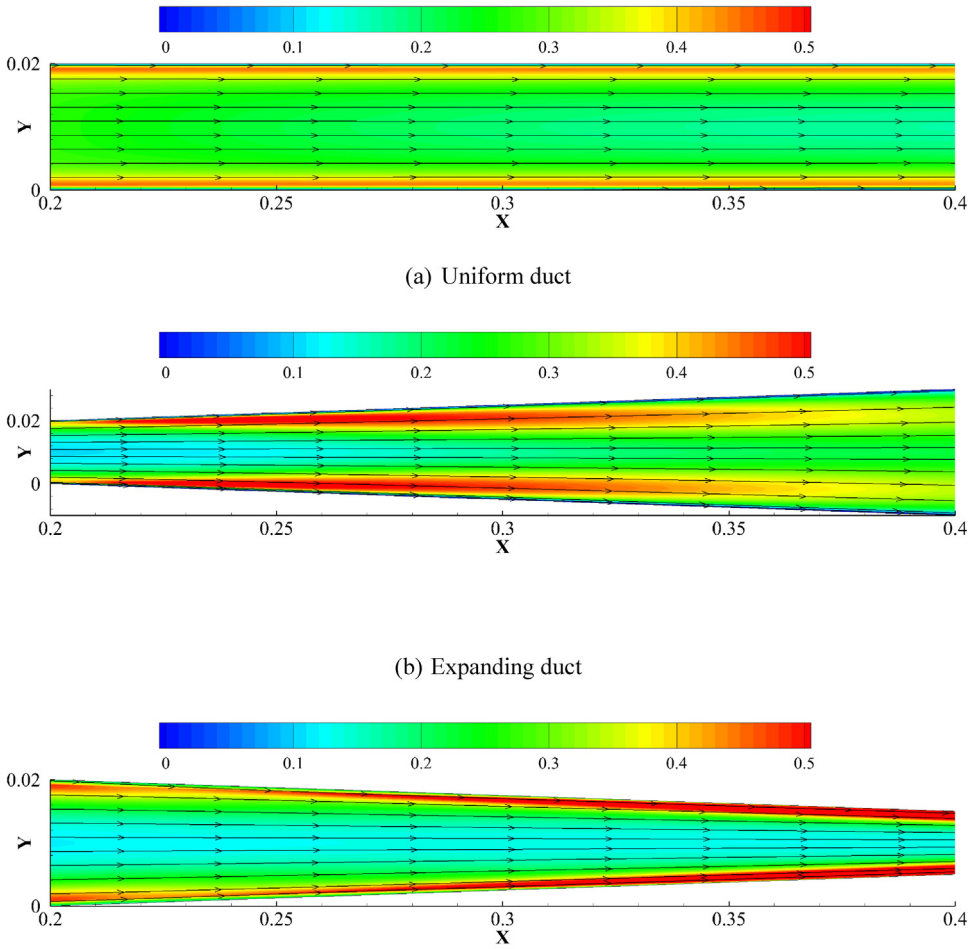

Fig. 10. T.K.E distribution and streamlines of air flow in uniform, expanding and contracting ducts.

2 The air flow field structures for varying section duct are significantly different with those of uniform duct case. Near-wall T.K.E. intensity and flow drags in expanding and contracting duct flow are greatly increased compared with uniform duct case.
3 For large particles ($d_p > 3\mu m$), the modified deposited distances and non-uniform air velocities in varying section ducts are the main mechanisms to change deposition rate compared with the uniform duct case. Nevertheless, the role of more intense near-wall turbulent motion and T.K.E. distribution is crucial for the deposition of small particles ($d_p < 3\mu m$) in varying section ducts.

In future work, the particle rebound and re-suspension from the wall need to be studied, as these may influence deposition rate of the particles.

Acknowledgement

The authors appreciate the financial supports provided by The Hong Kong Polytechnic University Postdoctoral Fellowships Scheme (G-YW0K) and Central Policy Unit of the Hong Kong Government via the Public Policy Research Scheme (2013.A6.010.13A).

References

[1] Q. Chen, Ventilation performance prediction for buildings: a method overview and recent applications, Build. Environ. 44 (4) (2009) 848–858.
[2] H. Lu, L. Lu, CFD investigation on particle deposition in aligned and staggered ribbed duct air flows, Appl. Therm. Eng. 93 (2016) 697–706.
[3] H. Lu, L. Lu, Numerical investigation on particle deposition enhancement in duct air flow by ribbed wall, Build. Environ. 85 (2015) 61–72.
[4] W. Hofmann, Modelling inhaled particle deposition in the human lung-a review, J. Aerosol Sci. 42 (2011) 693–724.
[5] B. Soni, S. Aliabadi, Large-scale CFD simulations of airflow and particle deposition in lung airway, Comput. Fluids 88 (2013) 804–812.
[6] W.S.J. Uijttewaal, R.V.A. Oliemans, Particle dispersion and deposition in direct numerical and large eddy simulations of vertical pipe flows, Phys. Fluids 8 (1996) 2590–2604.
[7] K. Sun, L. Lu, H. Jiang, A computational investigation of particle distribution and deposition in a 90° bend incorporating a particle-wall model, Build. Environ. 46 (2011) 1251–1262.
[8] H.H. Jin, J.R. Fan, M.J. Zeng, K.F. Cen, Large eddy simulation of inhaled particle deposition within the human upper respiratory tract, J. Aerosol Sci. 38 (2007) 257–268.
[9] H.H. Jin, C. He, L. Lu, J.R. Fan, Numerical investigation of the wall effect on airborne particle dispersion in a test chamber, Aerosol Air Qual Res 13 (2013) 786–794.
[10] M.I. Shapiro, M. Goldenberg, Deposition of glass fiber particles from turbulent air flow in a pipe, J. Aerosol Sci. 24 (1993) 65–87.
[11] G. Lecrivain, U. Hampel, Influence of the Lagrangian integral time scale estimation in the near wall region on particle deposition, ASME J. Fluids Eng. 134 (2012) 1–6.
[12] B.Y.H. Liu, J.K. Agarwal, Experimental observation of aerosol deposition in turbulent flow, J. Aerosol Sci. 5 (1974) 145–155.
[13] M.S. El-Shobokshy, Experimental measurements of aerosol deposition to smooth and rough surfaces, Atmos. Environ. 17 (1983) 639–644.
[14] K.W. Lee, J.A. Gieseke, Deposition of particles in turbulent pipe flows, J. Aerosol Sci. 25 (1994), 699–609.
[15] A.C. Wells, A.C. Chamberlain, Transport of small particles to vertical surfaces, Br. J. Appl. Phys. 18 (1967) 1793–1799.

[16] F. Fan, G. Ahmadi, A sublayer model for turbulent deposition of particles in vertical ducts with smooth and rough surfaces, J. Aerosol Sci. 24 (1993) 45–64.
[17] A.C.K. Lai, W.W. Nazaroff, Modelling indoor particle deposition from turbulent flow onto smooth surfaces, J. Aerosol Sci. 31 (2000) 463–476.
[18] B. Zhao, J. Wu, Modeling particle deposition from fully developed turbulent flow in ventilation duct, Atmos. Environ. 40 (2006), 457–446.
[19] B. Zhao, J. Wu, Modeling particle deposition onto rough walls in ventilation duct, Atmos. Environ. 40 (2006) 6918–6927.
[20] H. Lu, L. Lu, Effects of rib spacing and height on particle deposition in ribbed duct air flows, Build. Environ. 92 (2015) 317–327.
[21] N.P. Gao, J.L. Niu, Modeling particle dispersion and deposition in indoor environments, Atmos. Environ. 41 (2007) 3862–3876.
[22] H. Lu, L. Lu, A numerical study of particle deposition in ribbed duct flow with different rib shapes, Build. Environ. 94 (2015) 43–53.
[23] N.P. Gao, J.L. Niu, Q.B. He, T. Zhu, J.Z. Wu, Using RANS turbulence models and Lagrangian approach to predict particle deposition in turbulent channel flows, Build. Environ. 48 (2012) 206–214.
[24] H. Jiang, L. Lu, K. Sun, Simulation of particle deposition in ventilation duct with a particle-wall impact model, Build. Environ. 45 (5) (2010) 1184–1191.
[25] H. Jiang, L. Lu, K. Sun, Computational fluid dynamics (CFD) modelling of particle deposition in a two-dimensional turbulent channel air flow: study of influence factors, Indoor Built Environ. 21 (2) (2012) 264–272.
[26] K. Sun, L. Lu, H. Jiang, Modelling of particle deposition and rebound behaviour on ventilation ducting wall using an improved wall model, Indoor Built Environ. 20 (3) (2011) 300–312.
[27] M.B. Othmane, M. Havet, E. Gehin, C. Solliec, Mechanisms of particle deposition in ventilation ducts for a food factory, Aerosol Sci. Technol. 44 (2010) 775–784.
[28] F. Chorel, A. Kondjoyan, P.S. Mirade, Toward quantitative CFD prediction of contaminant particle deposition against surfaces in large forced-ventilation food plants, Aerosol Sci. Technol. 44 (2010) 10–28.
[29] B. Zhao, J.J. Chen, Numerical analysis of particle deposition in ventilation duct, Building Environ 41 (2006) 710–718.
[30] L. Tian, G. Ahmadi, Particle deposition in turbulent duct flows-comparisons of different model predictions, J. Aerosol Sci. 38 (2007) 377–397.
[31] Z. Zhang, Q. Chen, Prediction of particle deposition onto indoor surfaces by CFD with a modified Lagrangian method, Atmos. Environ. 43 (2009) 319–328.
[32] M.R. Sippola, W.W. Nazaroff, Modeling particle loss in ventilation ducts, Atmos. Environ. 37 (2003) 5597–5609.
[33] M.R. Sippola, W.W. Nazaroff, Experiment measuring particle deposition from fully developed turbulent flow in ventilation ducts, Aerosol Sci. Technol. 38 (2004) 914–925.
[34] M.R. Sippola, W.W. Nazaroff, Particle deposition in ventilation ducts: connectors, bends and developing turbulent flow, Aerosol Sci. Technol. 39 (2005) 139–150.
[35] S. Haber, D. Yitzhak, A. Tsuda, Characteristics of particle transport in an expanding or contracting alveolated tube, J. Appl. Physiol. 95 (2003) 657–671.
[36] D.Y. Lee, J.W. Lee, Characteristics of particle transport in an expanding or contracting alveolated tube, J. Aerosol Sci. 34 (2003) 1193–1215.
[37] J. Kim, P. Moin, R. Moser, Turbulence statistics in fully developed channel flow at low Reynolds number, J. Fluid Mech. 177 (1987) 133–166.
[38] A. Dehbi, A CFD model for particle dispersion in turbulent boundary layer flows, Nucl. Eng. Des. 238 (2008) 707–715.
[39] G. Lecrivain, S. Drapeau-Martin, T. Barth, U. Hampel, Numerical simulation of multilayer deposition in an obstructed channel flow, Adv. Powder Technol. 25 (2014) 310–320.
[40] B. Zhao, Y. Zhang, X.T. Li, X.D. Yang, D.T. Huang, Comparison of indoor aerosol particle concentration and deposition in different ventilated rooms by numerical method, Build. Environ. 39 (2004) 1–8.
[41] FLUENT Inc.: FLUENT 12.0 User's Guide. Lebanon, NH 2009.
[42] S.V. Partankar, Numerical Heat Transfer and Fluid Flow, Hemisphere, Washington, DC, 1980.
[43] N.B. Wood, A simple method for the calculation of turbulent deposition to smooth and rough surfaces, J. Aerosol Sci. 12 (1981) 275–290.
[44] S.K. Friedlander, H.F. Johnstone, Deposition of suspended particles from turbulent gas streams, Ind. Eng. Chem. 49 (1957) 1151–1156.
[45] A.K. Postma, L.C. Schwendiman, Studies in Micrometrics: I. Particle Deposition in Conduits as a Source of Error in Aerosol Sampling Report HW-65308, Hanford Laboratory, Richland, Washington, 1960.